# Unexpected Intermolecular C-H···O Hydrogen Bonds and <sup>1</sup>H NMR Chemical Shifts in a Key Linker for Fluorine-18 Labeling of Dimeric Drugs

Zelin Wang,† Bo Li,‡ Junfeng Wang,\*,¶ and Lu Wang\*,†

†Department of Chemistry and Chemical Biology, Institute for Quantitative Biomedicine,
Rutgers University, Piscataway, New Jersey 08854, USA

‡Department of Chemistry, Boston College, Chestnut Hill, Massachusetts 02467, USA

¶Gordon Center for Medical Imaging, Department of Radiology, Massachusetts General

Hospital, Harvard Medical School, Boston, Massachusetts 02114, USA

E-mail: jwang83@mgh.harvard.edu; lwang@chem.rutgers.edu

#### Abstract

The compound 2-(((trifluoromethyl)sulfonyl)oxy)propane-1,3-diyl bis(4-methylben-zenesulfonate) (TPB) is a crucial intermediate in the synthesis of <sup>18</sup>F radiolabeled cromolyn derivatives. In this work, we combine <sup>1</sup>H NMR spectroscopy, X-ray crystallography, ab initio molecular dynamics and NMR calculations to examine the structure, interactions and solvation dynamics of the TPB molecule. In CDCl<sub>3</sub>, the -CH<sub>2</sub> groups within its glyceryl-derived linker exhibit a single set of proton signals in the <sup>1</sup>H NMR measurements. However, when TPB is dissolved in DMSO-d<sub>6</sub>, distinct splitting patterns emerge despite its seemingly symmetric chemical structure. Crystallographic analysis further unveils the absence of overall symmetry in its three-dimensional arrangement. To elucidate these unique NMR features, we carry out ab initio molecular dynamics simulations and characterize the solvation structures and dynamics of TPB in

 $\mathrm{CHCl_3}$  and DMSO solutions. In contrast to the predominantly non-polar nature of the  $\mathrm{CHCl_3}$  solvents, DMSO directly participates in  $\mathrm{C\text{-}H\cdots}\mathrm{O}$  hydrogen bonding interactions with the solute molecule, leading to the splitting of its  $-\mathrm{CH_2}$  chemical shifts into two distinct distributions. The comprehensive understanding of the structure and solvation interactions of TPB provides essential insights for its application in the radiofluorination reactions of cromolyn derivatives and holds promise for the future development of radiolabeled dimeric drugs.

### Introduction

The synthesis of dimeric molecules has garnered significant attention over the past two decades. <sup>1,2</sup> This process, involving the combination of two identical molecules through a suitable linker, emerges as a promising strategy for developing effective drugs. Notably, the resulting dimers of biologically active molecules often exhibit increased activity compared to their monomeric counterparts, presenting a potential avenue to enhance drug effectiveness, broaden the biological spectrum, overcome resistance and improve pharmacological profiles. <sup>3–5</sup> Employing a bivalent ligand approach, these dimeric structures can also bridge independent recognition sites on transporters and foster favorable binding interactions. <sup>6</sup> This innovative strategy offers the potential for therapeutics with stronger responses than monomeric drugs, providing a novel direction in drug development. <sup>1,2,7–9</sup>

One example of such a molecule is cromolyn sodium 1, an FDA-approved medication em-

ployed for preventing mild to moderate bronchial asthma and providing additional treatment for allergic rhinitis and systemic mast cell disease (mastocytosis) in both pediatric patients and adults.<sup>10,11</sup> Recently, **1** was assessed for its impact on the fibrillization of the A $\beta$ 40 and A $\beta$ 42 peptides, revealing a remarkable inhibition of A $\beta$  fibril formation at a nanomolar concentration in vitro.<sup>12</sup> Additionally, in the transgenic APPswe/PS1 $\Delta$ E9 mouse model, significant and robust (>50%) reduction in soluble and insoluble A $\beta$  levels is observed just one week after in vivo intraperitoneal administration of **1**.<sup>12</sup> Combined with ibuprofen under the name ALZT-OP1, **1** went through a global Phase III clinical trial (Trial No. NCT02547818) by AZTherapies Inc. that is randomized, double-blinded, and placebo-controlled, focusing on subjects displaying early signs of Alzheimer's disease.

In the interim, a series of cromolyn derivatives were developed and evaluated. The fluorinated compound 2b proved to be the most effective derivative that led to a significantly increased uptake of A $\beta$ 42 in BV2 microglial cells in comparison to vehicle treatment. Furthermore, Shoup and coworkers radiolabeled the fluorinated cromolyn derivatives and evaluated their performance using positron emission tomography in vivo imaging. It is evident that compound 2a did not penetrate the blood-brain barrier, and the <sup>18</sup>F labeled 2b showed the best brain uptake (SUV >1 at 60 mins). <sup>13,14</sup> Consequently, we anticipate that prodrug **2b** could be a more effective candidate for therapy. The synthesis of [18F]2b starts with the precursor 3.15 As demonstrated in Figure 1, one might expect that directly substituting the tosylate group in 3 with a <sup>18</sup>F<sup>-</sup> ion would yield [<sup>18</sup>F]2b. Unexpectedly, this step proved challenging to perform, with no clear product observed even when heated at 120°C. Alternatively, Shoup and coworkers adopted a two-step labeling strategy for the successful synthesis of [18F]2b. 15 Using a key intermediate 2-(((trifluoromethyl)sulfonyl)ox-y)propane-1,3-diyl bis(4-methylbenzenesulfonate) (TPB), they performed the radiofluorination by substituting the triflate group, a more active leaving group than tosylate, with the <sup>18</sup>F<sup>-</sup> ion. The subsequent replacement of the two tosylate groups by 6 gave the targeted fluoro-radioactive cromolyn derivative [<sup>18</sup>F]**2b** (Figure 1).

TPB plays a critical role in synthesizing the cromolyn derivative [<sup>18</sup>F]**2b** and shows promise as a universal intermediate in dimeric drug production. We thus carried out a

Figure 1: Radiosynthesis of [<sup>18</sup>F]**2b** with TPB as a key intermediate for the radiofluorination process. Insets illustrate the chemical structures of the triflate and tosylate groups.

series of analyses and characterizations of the compound. To start, we synthesized TPB through a sequence of reactions as outlined in Figure S1. <sup>15</sup> The process initiated with the selective protection of two primary alcohol groups of glycerol using p-toluenesulfonyl chloride, resulting in 2-hydroxypropane-1,3-diyl bis(4-methylbenzenesulfonate). Subsequent reaction with trifluoromethanesulfonic anhydride yielded TPB (approximately 95% purity). We then investigated the reaction of TPB with the <sup>18</sup>F<sup>-</sup> ion and made a surprising discovery: using more than 5.0 mg of TPB yielded a pristine <sup>18</sup>F-labeled compound, whereas using less than 5.0 mg often produced two predominant radiolabeled compounds. This unexpected observation sparked our interest in the three-dimensional geometry of TPB. Initially, we expected TPB to possess C<sub>2</sub> symmetry based on its chemical structure in Figure 1. However, if the molecule lacked this symmetry, [<sup>18</sup>F]5 might not emerge as the major fluorinated product, potentially leading to a non-symmetric dimeric product (Figure 1).

To address this question, we conduct a comprehensive examination of TPB in this work. By combining <sup>1</sup>H NMR spectroscopy, X-ray diffraction, *ab initio* molecular dynamics (AIMD) simulations and NMR calculations, we will elucidate the structure, interactions and solvation dynamics of the molecule. These findings highlight the importance of precise structural characterization in ensuring the success and reliability of radiopharmaceutical syntheses. Therefore, they could serve as a cornerstone for the future development of radiolabeled dimeric drugs.

### Materials and Methods

#### <sup>1</sup>H NMR spectroscopy and X-ray crystallography measurements

All chemicals and solvents were purchased commercially and used without further purification. NMR spectra of TPB in two organic solvents, CDCl<sub>3</sub> and DMSO-d<sub>6</sub>, were recorded on a 500 MHz Varian spectrometer at 25°C. The chemical shifts are reported in the  $\delta$  scale in units of ppm, and the residual solvent peaks were used as the internal references.

X-ray crystallographic analysis was performed on selected single crystals of TPB for structural determination. The X-ray intensity data were measured at a temperature of 100(2) K (Oxford Cryostream 700) on a Bruker Kappa APEX Duo diffractometer system equipped with a sealed Mo-target X-ray tube ( $\lambda = 0.71073$  Å). The crystals were mounted on a goniometer head with paratone oil. The detector was placed at a distance of 5.000 from the crystal. Data collection strategy was determined by the APEX software and all frames were collected with a scan width of  $0.5^{\circ}$  in  $\omega$  and  $\phi$ , with an exposure time of 10 or 20 s/frame.

The frames were integrated with the Bruker SAINT Software using a narrow-frame integration algorithm to a maximum  $2\theta$  angle of  $56.54^{\circ}$  (0.75 Å resolution). The final cell constants are based upon the refinement of the XYZ-centroids of several thousand reflections above  $20 \sigma(I)$ . Analysis of the data showed negligible decay during data collection. Data were corrected for absorption effects using the empirical method (SADABS). The structures were solved and refined by full-matrix least squares procedures on  $|F^2|$  using the Bruker

SHELXTL software (version 6.12). All hydrogen atoms were included in idealized positions for structure factor calculations except for those forming hydrogen bonds or on a chiral center. Anisotropic displacement parameters were assigned to all non-hydrogen atoms except those displaying disorder.

#### Computational methods

Classical molecular dynamics (MD) simulations and AIMD simulations were conducted to explore the geometry fluctuations of TPB in CHCl<sub>3</sub> and DMSO solutions. CHCl<sub>3</sub> and DMSO were used as solvents instead of CDCl<sub>3</sub> and DMSO-d<sub>6</sub> because the H and D atoms share the same electronic structure and the difference in their atomic masses is expected to have minimal influence on solute-solvent interactions and the resulting <sup>1</sup>H chemical shifts of TPB.

MD simulations were performed using the Amber 2020 software and the intra and intermolecular interactions were modeled using the general Amber force field.  $^{16,17}$  To set up the systems, the crystal structure of TPB was solvated in rectangular boxes containing 117 CHCl<sub>3</sub> or 100 DMSO molecules. Following energy minimization, each solution was equilibrated under the NPT condition for 5 ns. The simulation temperature was maintained at 300 K using the Langevin thermostat with a collision frequency of 2 ps<sup>-1</sup>, and the pressure was kept at 1 atm using the Berendsen barostat with a relaxation time of 1 ps.  $^{18,19}$  The resulting box sizes were  $24.3 \times 25.9 \times 26.2 \text{ Å}^3$  for the CHCl<sub>3</sub> solution and  $21.8 \times 23.4 \times 24.0 \text{ Å}^3$  for the DMSO solution. The systems were then equilibrated under a constant temperature of 300 K for 5 ns. In all simulations, the structure of TPB was fixed using positional restraints with a force constant of  $10.0 \text{ kcal/mol/Å}^2$ . The simulations were performed with a time step of 2 fs and chemical bonds involving hydrogen atoms were constrained using the SHAKE algorithm.  $^{20}$ 

Starting with the equilibrated structures from MD simulations, we performed AIMD simulations of TPB in CHCl<sub>3</sub> and DMSO solutions. The Quickstep module in the CP2K package was used for on-the-fly electronic structure evaluations, and the i-PI package was

employed for propagating the nuclear motion. <sup>21,22</sup> The CHCl<sub>3</sub> and DMSO solutions contained 637 and 1052 atoms, respectively, and the electronic structure was described using the BLYP density functional and the D3 dispersion correction. <sup>23–25</sup> Core electrons were represented using the Goedecker-Teter-Hutter pseudopotentials, while valence charge densities of the systems were described using the DZVP-GTH plane-wave basis set with a cutoff of 400 Rydberg. <sup>26,27</sup> The AIMD simulations were performed in the NVT ensemble for 60 ps with a time step of 0.5 fs. Velocity rescaling was applied every 10 fs to maintain the simulation temperature at 300 K. <sup>28</sup> The initial 10 ps of the simulations were used for equilibration, and the remaining 50 ps of the trajectory were subjected for further analysis.

From the AIMD simulations, we obtained representative TPB structures and calculated the isotropic shielding constants of the H atoms,  $\sigma$ , using the Gauge-Independent Atomic Orbital (GIAO) method as implemented in the Gaussian 16 package. <sup>29–34</sup> The calculations were performed with the B3LYP density functional, the D3 dispersion correction and the triple- $\zeta$  6-311+G(2d,p) basis set. <sup>23,25,35,36</sup> We selected this combination of the DFT method and basis set for its proven accuracy in predicting <sup>1</sup>H and <sup>13</sup>C NMR chemical shifts for organic molecules.  $^{37-39}$  In the CHCl $_3$  solution, we collected 2001 TPB configurations at an interval of 25 fs from the AIMD simulations. For the DMSO solution, we extracted TPB-DMSO clusters every 25 fs from the AIMD simulations to incorporate solute molecules involved in C-H···O hydrogen bonds with the solute. The polarizable continuum model (PCM) was applied to mimic the solution environment, using a dielectric constant of 4.7 for CHCl<sub>3</sub> and 46.8 for DMSO. An intermolecular C-H···O hydrogen bond was considered present if the C-O distance  $d_{CO} < 4.0$  Å and the C-H-O angle  $\theta_{CHO} > 110^{\circ}$ . Benchmark NMR calculations were preformed to validate our selection of implicit or hybrid solvent models in the NMR calculations, as detailed in the Supporting Information. The proton shielding constants of the reference molecule tetramethylsilane,  $\sigma_{TMS}$ , were calculated to be 31.94 and 31.93 ppm in CHCl<sub>3</sub> and DMSO solutions, respectively, using the PCM model. For every snapshot generated from the AIMD simulations, the chemical shifts of a proton in the TPB molecule was derived from  $\sigma_{TMS} - \sigma$  in the corresponding solvent. We then computed the distribution of the 2001 <sup>1</sup>H chemical shifts for each solution, and fitted them with one or two Gaussian functions to obtain the final chemical shifts (Figure S6).

Natural Bond Orbital (NBO) analysis was performed to evaluate the intermolecular C-H···O hydrogen bond formed between the  $-\mathrm{CH}_2$  group of TPB and DMSO using the Gaussian 16 and NBO6 packages. <sup>34,41</sup> After optimizing the molecular geometries, we conducted NBO analysis on an isolated TPB molecule and a TPB-DMSO hydrogen bonded pair in vacuum with the B3LYP density functional and 6-31G(d) basis set. Orbital visualization was carried out using the Jmol software. <sup>42</sup> More analyses are provided in the Supporting Information.

### Results and Discussion

#### Distinct <sup>1</sup>H NMR spectra and crystal structure of TPB

In CDCl<sub>3</sub> solution, TPB presents five distinct sets of proton signals in its <sup>1</sup>H NMR spectrum with chemical shifts,  $\delta_H$ , spanning from 2 to 8 ppm (Table 1 and Figure S3a). Reflecting its chemical structure, which contains a triflate group nestled between two tosylate groups via a glyceryl-derived linker, the H atoms of TPB reside in 5 distinct chemical environments:  $-CH_3$ ,  $-CH_2$ , -CH, and the meta- and ortho-positions on the two aromatic rings. The  $-CH_3$  groups display a singlet peak with a high-field  $\delta_H$  value of 2.48 ppm, consistent with the strong shielding effect within the terminal methyl of the tosylate groups. In contrast, the meta- and ortho-H atoms on the aromatic rings experience diminished shielding, leading to  $\delta_H$  values of 7.39 and 7.77 ppm, respectively, and spin-spin coupling with the adjacent proton induces the splitting of these peaks into doublets. Between these signals, we observe one set of proton signals for the alkyl  $-CH_2$  and -CH groups within the glyceryl-derived linker, displaying  $\delta_H$  values of 4.23 and 5.09 ppm, respectively. Their peaks manifest as doublets and quintets, arising from spin-spin coupling with nearby protons. The integrated peak areas, arranged from high to low fields, maintain a ratio of 6:4:1:4:4 going and align

well with the anticipated distribution of H atoms in each chemical environment. Thus the spectral features observed in the <sup>1</sup>H NMR analysis strongly indicate a symmetric structure of the TPB molecule.

Table 1: Chemical shifts, splitting patterns and integrated peak areas for the 5 types of H atoms in the <sup>1</sup>H NMR spectra of TPB in CDCl<sub>3</sub> and DMSO-d<sub>6</sub>. The 5 types of H atoms are labeled in Figure S2.

| H atoms           | $\mathrm{CDCl}_3$        |           |      | $\mathrm{DMSO}	ext{-}\mathrm{d}_6$ |           |      |
|-------------------|--------------------------|-----------|------|------------------------------------|-----------|------|
|                   | $\delta_H \text{ (ppm)}$ | Splitting | Area | $\delta_H \text{ (ppm)}$           | Splitting | Area |
| $-CH_3$           | 2.48                     | singlet   | 6.5  | 2.44                               | singlet   | 6.4  |
| $-\mathrm{CH}_2$  | 4.23                     | doublet   | 4.5  | 4.17                               | multiplet | 2.2  |
|                   |                          |           |      | 4.30                               | multiplet | 2.1  |
| -CH               | 5.09                     | quintet   | 1.0  | 5.01                               | multiplet | 1.0  |
| $-C_6H_4$ (meta)  | 7.39                     | doublet   | 4.4  | 7.52                               | doublet   | 4.4  |
| $-C_6H_4$ (ortho) | 7.77                     | doublet   | 4.3  | 7.80                               | doublet   | 4.3  |

Surprisingly, TPB demonstrates complex splitting patterns in the  $^{1}$ H NMR spectrum when it is dissolved in DMSO-d<sub>6</sub> solution (Table 1 and Figure S3b). While the NMR signals remain similar for the  $-\text{CH}_3$  and aromatic moieties, the  $-\text{CH}_2$  resonance manifests as two discernible peaks at  $\delta_H$  values of 4.17 and 4.30 ppm, respectively. Each peak appears as a doublet of doublets and their integrated areas are approximately equal, strongly suggesting that the H atoms in each  $-\text{CH}_2$  group occupy two distinctive chemical environments. Furthermore, the -CH signal appears at  $\delta_H$  of 5.01 pm and also shows complex splitting features. The integrated peak areas follow a ratio of 6:4:1:4:4 in accordance with the molecular composition. In contrast to the behavior observed in CDCl<sub>3</sub> solution, the NMR analysis in DMSO-d<sub>6</sub> suggests that the TPB molecule may adopt an asymmetric configuration despite its apparent symmetric chemical structure. The intricate splitting patterns deepen the mystery surrounding the structure of TPB and its reactions with the  $^{18}\text{F}^-$  ion, as illustrated in Figure 1.

To resolve the seemingly contradicting observations in the <sup>1</sup>H NMR measurements, we perform X-ray diffraction to determine the crystal structure of TPB. As illustrated in Figure 2, TPB indeed exhibits an absence of symmetry in its three-dimensional structure. In

the crystalline phase, the central triflate group points towards one side, while the two to-sylate rings adopt asymmetric orientations with a dihedral angle of  $78.5^{\circ}$ . These geometric arrangements dictate that the four H atoms in the  $-\text{CH}_2$  groups reside in two distinct chemical environments. H1 and H3 are oriented inward in the molecule and almost parallel to the tosylate rings, with angles between the C-H bonds and the normal vectors of the rings measuring  $96.4^{\circ}$  and  $93.9^{\circ}$ , respectively. The distances from these two atoms to the geometric centers of the aromatic rings,  $d_{HX}$ , are closely situated at 3.3 Å and 3.7 Å, respectively. In contrast, the H2 and H4 atoms are exposed outward from the molecule and positioned in proximity to the O atoms of the sulfonate groups. Their distances to the closest O atoms,  $d_{HO}$ , amount to 2.70 Å and 2.75 Å, and the C-H-O angles are  $92.8^{\circ}$  and  $87.8^{\circ}$ , respectively.

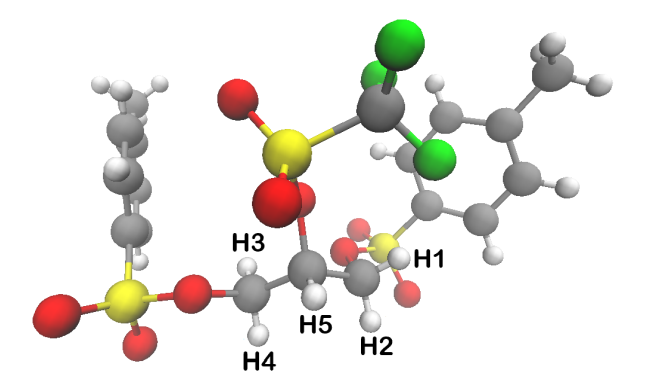


Figure 2: X-ray crystallographic structure of TPB with H atoms in the glyceryl-derived linker labeled. Grey, red, yellow, green and white represent C, O, S, F and H atoms, respectively.

# Structures and solvation for TPB in CHCl<sub>3</sub> and DMSO solutions

To comprehensively understand the distinctive features observed in the <sup>1</sup>H NMR spectra, we carry out a series of electronic structure analysis and examine the chemical shifts and solvation structures of TPB. We start with the crystal structure of TPB and evaluate its chemical shifts in the gas phase. As listed in Table S1, the calculated  $\delta_H$  values are in reasonable agreement with experimental measurements, showing deviations ranging between 0.05 and 1.25 ppm. However, each H atom has a different chemical shift owing to the asymmetric nature of the molecular structure, and this phenomenon persists even when the

TPB molecule is placed in CHCl<sub>3</sub> and DMSO solutions using the PCM model. The presence of additional NMR peaks is inconsistent with experimental data and arises from the lack of dynamical fluctuations in the TPB structure induced by solute-solvent interactions. In other words, calculations based on a static TPB configuration are not sufficient to capture the observed chemical shifts and their solvent dependence in the <sup>1</sup>H NMR spectroscopy experiments.

We then perform AIMD simulations for the TPB molecule in both  $CHCl_3$  and DMSO solutions to assess the influence of solvation structures and configurational fluctuations on the  $^1H$  NMR chemical shifts. These first-principles simulations dynamically solve the Schrödinger equation, explicitly incorporating electronic many-body effects and solute-solvent interactions without relying on pre-defined parameters.  $^{43}$  Despite their high computational cost, these simulations have been widely adopted to incorporate dynamical effects in predicting NMR properties, including  $^1H$ ,  $^{13}C$  and  $^{15}N$  chemical shifts.  $^{44-48}$  Throughout the AIMD simulations, TPB maintains its structural characteristics observed in the crystal phase, with the H1 and H3 atoms proximal to the aromatic rings and the H2 and H4 atoms close to the O atoms in the tosylate groups. To characterize the configuration of TPB, we use  $d_{HX}$  and  $d_{HO}$  as geometric parameters and calculate the free energies as

$$F = -k_B T ln \frac{P(d_{HO}, d_{HX})}{P_{max}}. (1)$$

Here  $k_B$  is Boltzmann constant and T is the simulation temperature.  $P(d_{HO}, d_{HX})$  is the probability of observing the  $-\text{CH}_2$  groups in the  $(d_{HO}, d_{HX})$  configuration, and  $P_{max}$  is the probability of finding the TPB molecule at its most favorable configuration.

As depicted in Figure 3,  $P_{max}$  occurs at  $d_{HO}$  of 2.6 Å and  $d_{HX}$  of 3.6 Å in the CHCl<sub>3</sub> solution. The TPB molecule undergoes relatively free fluctuations when the two distances are in the range of 2.3 - 3.2 Å and 3.1 - 4.2 Å, respectively, with a free energy cost of less than 1 kcal/mol. The observed  $d_{HO}$  values are primarily below the sum of the van der Waals radii

of the H and O atoms (2.7 Å), <sup>49</sup> and the simulations indicate a 5.5% probability of observing an intramolecular C-H···O hydrogen bond. In the DMSO solution, TPB predominantly takes a configuration with  $d_{HO}$  at 2.8 Å and  $d_{HX}$  at 3.4 Å, and these distances fluctuate between 2.4-3.3 Å and 3.0-4.0 Å, respectively. Compared to CHCl<sub>3</sub>, the likelihood of forming an intramolecular C-H···O hydrogen bond reduces to 0.7%, indicating that TPB adopts a less compact conformation with the tosylate groups moving away from the glyceryl-derived linker. From Figure 3, the TPB molecule exhibits a more flexible structure in the CHCl<sub>3</sub> solution as it explores a larger phase space than in the DMSO solution.

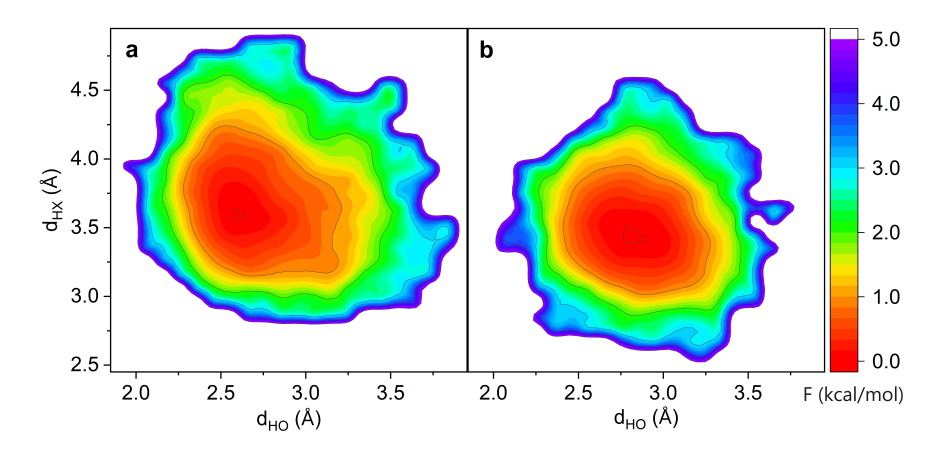


Figure 3: Free energy surfaces of TPB in (a) CHCl<sub>3</sub> and (b) DMSO solutions obtained from AIMD simulations.

Given the importance of solute-solvent interactions, we examine the solvation structure of TPB by calculating the radial distribution functions between its H atoms and the Cl atom in CHCl<sub>3</sub> or the O atom in DMSO. As shown in Figure S7, CHCl<sub>3</sub> molecules are loosely arranged around TPB with the electronegative chlorine atoms oriented towards the solute H atoms. The first peak in the radial distributions function is observed at an H-Cl distance of 3.2 Å, characterized by a relatively weak intensity of 1.04. Focusing on the linker  $-CH_2$  groups (Figure 4a), the first peak appears at 3.0 Å, which approximately matches the sum of the van der Waals radii of the H and Cl atoms. H1 and H3 are positioned inward in the TPB molecule and exhibit lower solvent accessibility, resulting in peak intensities below 1. Conversely, H2 and H4 point towards the solvent, displaying peak intensities around 1.1.

The first solvation shell is observed at an H-Cl distance of 4.0 Å, incorporating an average of  $0.9 \text{ CHCl}_3$  solvent molecules around each  $-\text{CH}_2$  group.

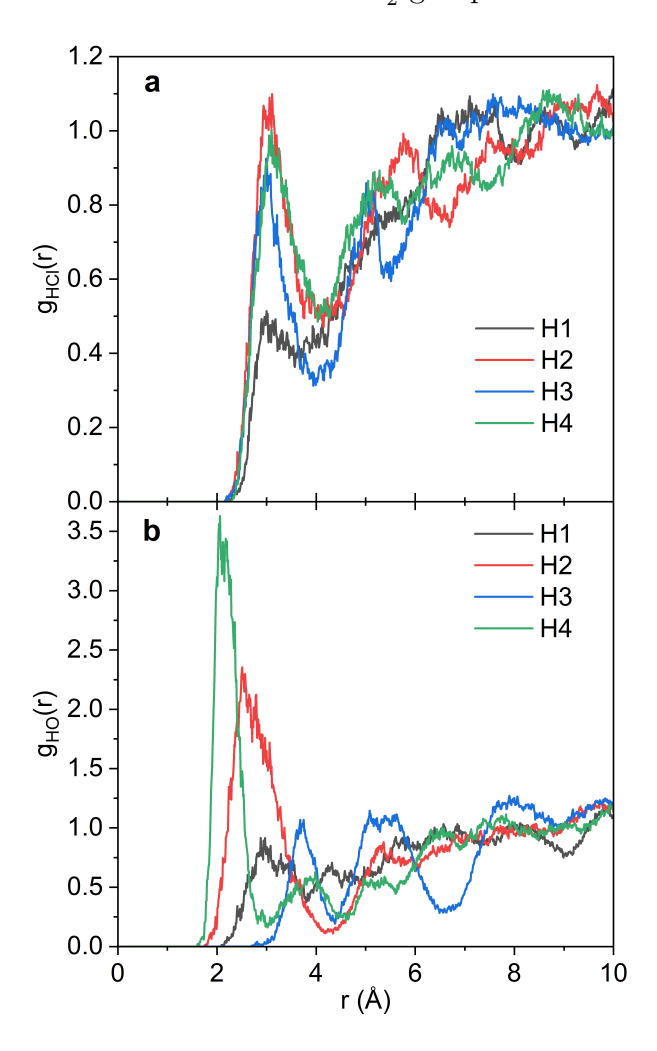


Figure 4: Radial distribution functions between the  $-\mathrm{CH}_2$  groups of TPB and (a) the Cl atom in CHCl<sub>3</sub> and (b) the O atom in DMSO from the AIMD simulations.

Unlike the  $\mathrm{CHCl_3}$  solution, the DMSO molecules demonstrate more organized solvation layers where their O atoms form characteristic arrangements around the solute H atoms. In Figure S7, the H-O radial distribution function reveals a primary peak at 2.4 Å and a second peak at 3.9 Å . Zooming in on the  $-\mathrm{CH_2}$  groups, H1 and H3 adopt inward-facing geometries and are largely shielded from the solvents (Figure 4b). In contrast, H2 and H4 display prominent peaks at H-O distances of 2.6 and 2.1 Å, respectively, indicating a close proximity within the sum of their van der Waals radii. This observation, combined with the calculated

average  $d_{CO}$  of 3.4 Å and  $\theta_{CHO}$  of 134° from the AIMD trajectories, strongly indicates the presence of solute-solvent C-H···O hydrogen bonds. Indeed, we observe significant probabilities of 83.5% and 97.1% for H2 and H4 to form a C-H···O hydrogen bond with surrounding DMSO molecules, respectively. These H atoms further show probabilities of 3.3% and 2.4% of participating in two hydrogen bonds with the solvents. Beyond the  $-\text{CH}_2$  groups, each  $-\text{CH}_1$ , and the ortho- and meta-H atoms participates in an average of 1.0, 0.7, 0.9 and 0.6 intermolecular C-H···O hydrogen bonds, respectively.

Intriguingly, AIMD simulations reveal that the  $-\mathrm{CH}_2$  and  $-\mathrm{CH}$  groups in the glycerylderived linker have heightened propensities to form hydrogen bonding interactions with the solvent DMSO, surpassing other H-containing functional groups in TPB. Using the PCM model to describe the DMSO solvation environment, we carry out Mulliken population analysis and find that the H atoms in these two functional groups bear partial charges of  $\sim 0.20$ , which are the highest among all H atoms (Table S1). This electron deficiency enhances the accessibility of these atoms, in particular H2, H4 and H5, to electron donors in the solvent environment. The intricate interaction patterns between TPB and the DMSO solvents, along with their dynamical fluctuations, collectively induce structural alternation in the solute molecule. As demonstrated in Figure 3, this manifests as a shift towards a more open configuration and a noticeable reduction in intramolecular C-H···O hydrogen bonds in the DMSO solution as compared to the CHCl<sub>3</sub> solution.

# Splitting patterns in the <sup>1</sup>H NMR spectra of TPB

From the AIMD simulations, we extract 2001 representative configurations of TPB or TPB-DMSO clusters and carry out electronic structure calculations to determine their  $^{1}$ H NMR chemical shifts. As depicted in Figure S6, the  $\delta_{H}$  values for a given functional group typically follow a symmetric distribution and can be modeled using a Gaussian function. These distributions, which span a range of 1 – 3 ppm, arise from fluctuations in the TPB configuration and its local solvation environment. Compared to CHCl<sub>3</sub>, the  $\delta_{H}$  distributions

are broader in the DMSO solution, indicating an increased degree of heterogeneity in the solvation structures. This is particularly the case for the  $-CH_2$  group in the glyceryl-derived linker, whose  $\delta_H$  distribution exhibits a shoulder in addition to the main peak in the DMSO solution. We thus apply two Gaussian functions to fit its distribution curve, each representing distinct chemical environments surrounding the H atoms. The positions and intensities of the calculated NMR peaks are determined by the centers and areas of the Gaussian fits, respectively (Table S2). Note that spin-spin couplings are omitted in these calculations.

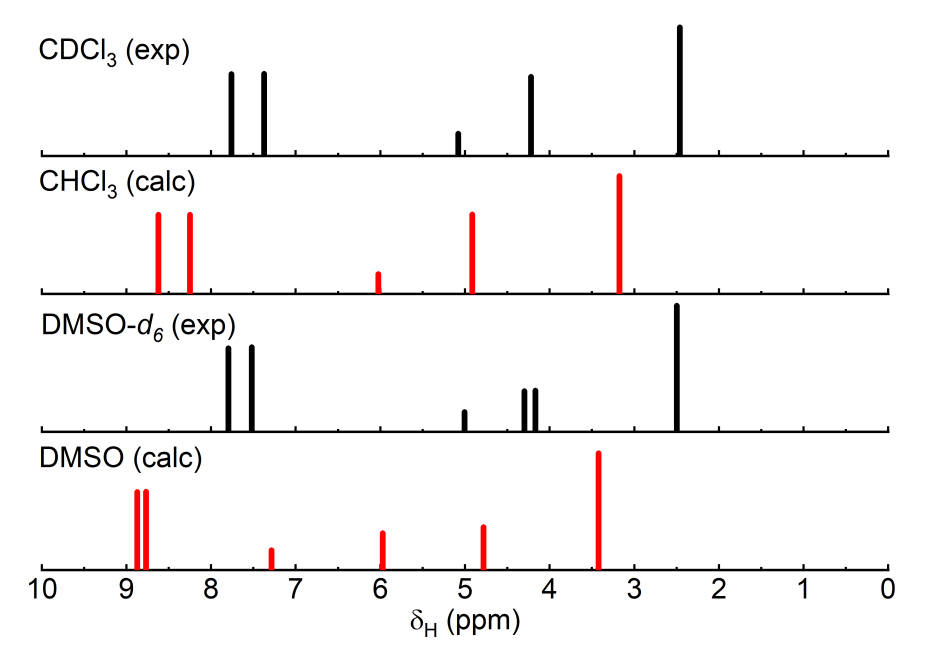


Figure 5: Experimental and calculated <sup>1</sup>H NMR chemical shifts of TPB in organic solvents. Intensities of the calculated peaks are proportional to the integrated areas of their corresponding peaks.

As demonstrated in Figure 5, the calculated NMR features correctly capture the trends observed in the experimental data. When TPB is dissolved in the CHCl<sub>3</sub> solution, we find 5 distinct NMR signals that correspond to the 5 types of H-containing functional groups in the TPB molecule. Among them, the terminal methyl groups contain the most shielded H atoms with a  $\delta_H$  value of 3.18 ppm. The chemical shifts for  $-\text{CH}_2$  and -CH in the glyceryl-derived linker are comparatively higher at 4.93 and 6.03, respectively. In contrast, H atoms in the meta- and ortho-positions on the tosylate rings are much less shielded, displaying downfield

 $\delta_H$  values of 8.26 and 8.63 ppm, respectively. The predicted chemical shifts consistently surpass the experimental values by 0.7 – 0.9 ppm due to systematic errors in the electronic structure methods and implicit solvent model applied in the NMR calculations. The importantly, both the number and intensity of the NMR peaks align closely with experimental data. Within a specific functional group, H atoms exhibit a single NMR signal as the TPB configuration fluctuations and CHCl<sub>3</sub> solvation dynamics create, on average, a homogeneous chemical environment around them.

In the DMSO solution, our NMR calculations reveal the presence of 6 distinctive peaks (Figure 5). The  $-CH_3$  groups remain the most shielded, displaying a  $\delta_H$  of 3.47 ppm, whereas the meta- and ortho-H atoms on the aromatic rings are the most deshielded with chemical shifts of 8.81 and 8.90 ppm, respectively. Notably, the  $-CH_2$  groups now exhibit two peaks at 4.77 and 5.97 ppm with an intensity ratio of 1.1, in good agreement with experimental findings. To elucidate the origin of this distinctive dual-peak feature, we decompose the  $\delta_H$  distribution based on the hydrogen bonding conditions of the  $-\mathrm{CH}_2$  groups. As shown in Figure 6, the two distributions exhibit peaks at 4.70 and 5.95 ppm, respectively, with comparable integrated areas, in excellent agreement with the predicted NMR features. When H atoms are devoid of intermolecular hydrogen bonds, they display a smaller chemical shift and a narrower  $\delta_H$  distribution. Conversely, when the H2 and H4 atoms are involved in 1 or 2 intermolecular C-H···O hydrogen bonds with the DMSO solvents, they become considerably deshielded with more downfield chemical shifts. Dynamic structural rearrangements in the solvation shells create a heterogeneous environment around H2 and H4, resulting in the broadening of their  $\delta_H$  distributions. We further conduct NBO analysis to characterize how electron redistribution influences the observed chemical shifts in the absence and presence of an intermolecular C-H···O hydrogen bond. As illustrated in Figure 7a, the  $\sigma_{CH}$  orbital is localized in the linker  $-CH_2$  group when TPB is in an isolated state. The covalent C-H bond strongly shields the proton, resulting in a smaller  $\delta_H$  value. Upon formation of an intermolecular C-H···O hydrogen bond, the antibonding  $\sigma_{CH}^*$  orbital in the linker  $-\text{CH}_2$  group overlaps with the p-type lone pair orbital,  $n_p$ , of the O atom in DMSO (Figure 7b). This overlap leads to a  $n_p \to \sigma_{CH}^*$  electron transfer, weakening the corresponding C-H bond and shifting its  $\delta_H$  value downfield. Therefore, the two-peak feature of the  $-\text{CH}_2$  group originates from its hydrogen bonding interactions with the solvent molecules. Although C-H···O hydrogen bonds are much weaker than canonical hydrogen bonds that involve O, N or F atoms, they exert a significant influence on the chemical environment surrounding the linker  $-\text{CH}_2$  groups. <sup>1</sup>H NMR proves to be highly sensitive to discern their effects on the electronic distributions in the TPB molecule.

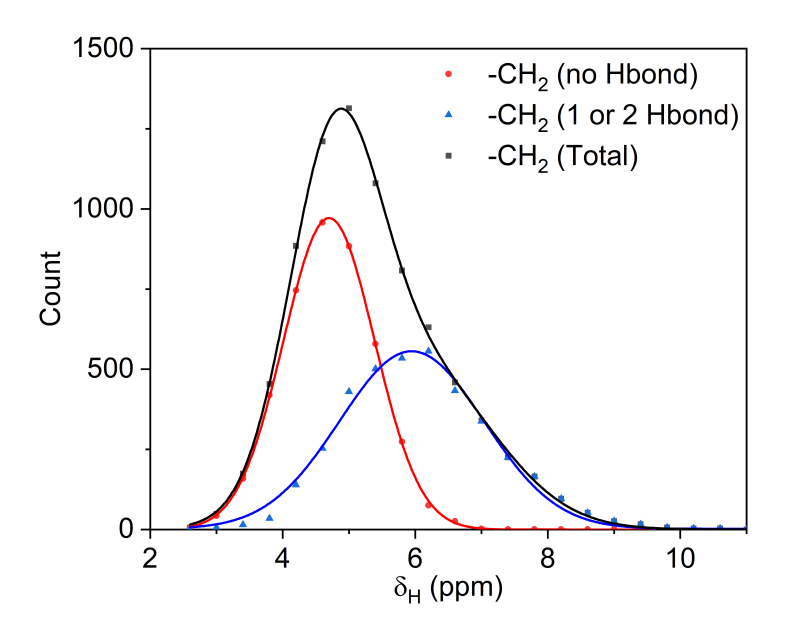


Figure 6: Distribution and decomposition of  $-CH_2$  chemical shifts for TPB in DMSO solution. Black squares depict the overall  $\delta_H$  distribution, and red dots and blue triangles represent the distributions in the absence and presence of intermolecular C-H···O hydrogen bonds, respectively. Gaussian functions are applied to fit the corresponding  $\delta_H$  distributions (lines).

Within the glyceryl-derived linker of TPB, the H5 atom in the -CH group is also predicted to have a downfield chemical shift of 7.26 ppm in DMSO solution (Figure 5). From the AIMD trajectories, the -CH group shows a 98.6% probability of forming at least one C-H···O hydrogen bond with the solvent molecules. Compared to the -CH<sub>2</sub> groups, -CH

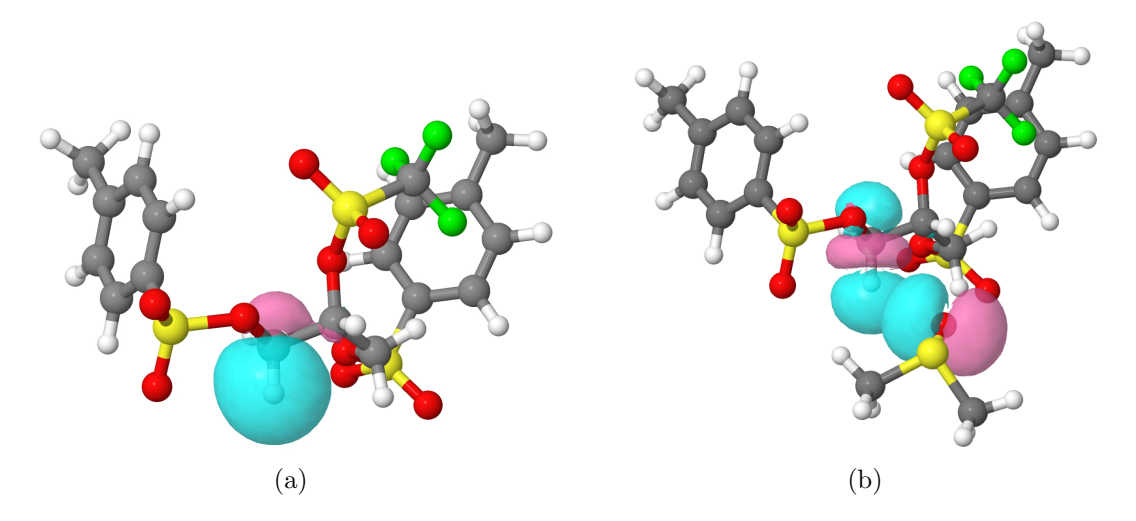


Figure 7: Natural bond orbitals of TPB. (a) The  $\sigma_{CH}$  orbital of a  $-\text{CH}_2$  group in an isolated TPB molecule. (b) The overlap of the  $\sigma_{CH}^*$  and  $n_p$  orbitals when TPB is hydrogen bonded to a DMSO solvent. Grey, red, yellow, green and white represent C, O, S, F and H atoms, respectively. The pink and cyan spheres depict the positive and negative molecular orbitals at an isovalue of 0.03.

forms shorter and more linear intermolecular hydrogen bonds, characterized by an average  $d_{CO}$  of 3.2 Å and  $\theta_{CHO}$  of 140°. To comprehensively assess the interactions between the glyceryl-derived linker of TPB and DMSO solvents, we collectively examine the H2, H4 and H5 atoms and calculate their proton sharing coordinates,  $\nu = d_{CH} - d_{OH}$ , in the intermolecular C-H···O hydrogen bonds. As shown in Figure 8,  $\nu$  consistently takes negative values throughout the AIMD simulations as the protons remain covalently bonded to the C atom in the weak C-H···O hydrogen bonds. At a given simulation step, the instantaneous  $\delta_H$  is strongly dependent on the proton positions and undergoes a three-fold increase as the proton becomes more shared in the hydrogen bond, with  $\nu$  changing from -2.3 Å to -0.5 Å. From Figure 8,  $\delta_H$  of H2, H4 and H5 follows a universal trend despite the fact that these atoms belong to separate functional groups in TPB. This observation suggests that  $\nu$  serves as an effective coordinate linking the geometry of a hydrogen bond to the electron distribution and chemical shielding on the protons, in good agreement with previous findings from first-principles simulations and NMR calculations  $^{46,50,51}$ 

Based on the AIMD simulations, the distinctive features observed in the <sup>1</sup>H NMR spec-

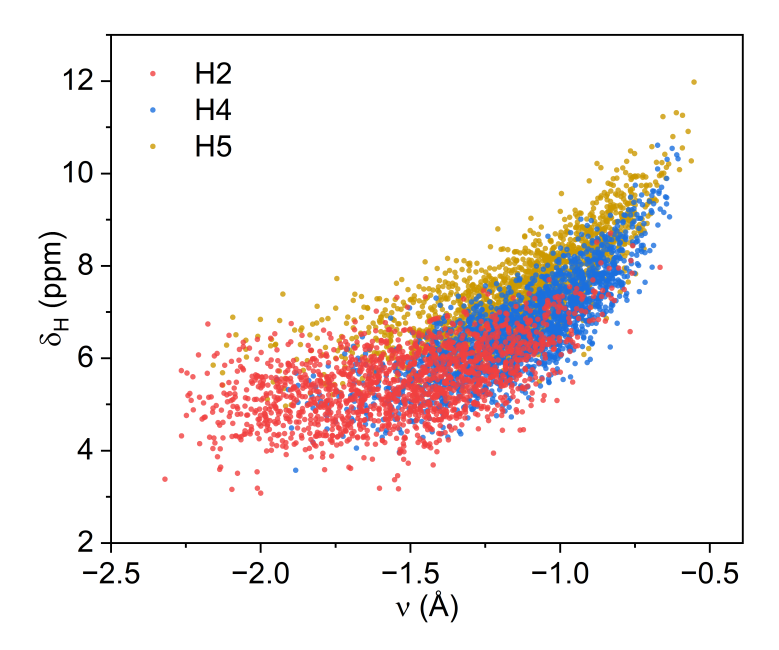


Figure 8: Instantaneous chemical shifts of the H2, H4 and H5 atoms as a function of the proton sharing coordinate  $\nu$  when they are involved in solute-solvent C-H···O hydrogen bonds. Each dataset comprises 2001 points sampled from the AIMD simulations.

troscopy experiments arise from the unique solvation conditions of CHCl<sub>3</sub> and DMSO surrounding the TPB molecule. In the CHCl<sub>3</sub> solution, solvent molecules lack the ability to engage in hydrogen bonding interactions, and TPB adopts a more compact geometry with the H2 and H4 atoms showing a 5.5% probability of forming intramolecular C-H···O hydrogen bonds with the tosylate O atoms (Figure 3a). While TPB assumes an asymmetric structure, the dynamical fluctuations of its configuration and the solvation structures, on average, create a homogeneous environment surrounding the solute H atoms, giving rise to five distinct proton signals in the  $^{1}$ H NMR spectrum. In the DMSO solution, the alkyl and aromatic functional groups participate in intermolecular C-H···O hydrogen bonds with the solvents, distorting the TPB geometry and reducing the probability of forming intramolecular C-H···O hydrogen bonds to 0.7% (Figure 3b). These specific solute-solvent interactions further split the  $-\text{CH}_2$  NMR signal into two peaks wherein the hydrogen-bonded H2 and H4 atoms exhibit more downfield chemical shifts compared to the solvent-shielded H1 and H3 atoms, resulting in a total of six proton signals in the NMR spectrum.

Note that in Figure 5, the calculated chemical shifts of TPB consistently exceed the

experimental values in DMSO by 0.6 – 2.3 ppm, with the linker –CH and –CH<sub>2</sub> groups showing the most substantial difference. In addition to the intrinsic errors of the chosen electronic structure methods, these discrepancies are primarily attributed to the limited sampling of configurational fluctuations and solvation dynamics within the brief 50-ps AIMD simulations. Additionally, the first few solvation shells of TPB may collectively influence its predicted <sup>1</sup>H chemical shifts. However, the current calculations explicitly incorporate only DMSO molecules directly involved in hydrogen bonding interactions with TPB, while the remainder of the solution is treated using the PCM model to maintain computationally feasibility. Despite these considerations, the correct reproduction of both the number and intensity of the experimental NMR peaks by the predicted <sup>1</sup>H chemical shifts supports the validity of our qualitative assessments.

# Conclusion

In this work, we conduct a joint experimental and computational investigation into the structure and <sup>1</sup>H NMR spectra of TPB, a key intermediate molecule in the synthesis of <sup>18</sup>F radiolabeled cromolyn derivatives. In the non-polar solvent CHCl<sub>3</sub>, TPB displays five sets of proton signals in the <sup>1</sup>H NMR spectrum, each corresponding to a distinct H-containing functional group. Conversely, when dissolved in DMSO, the molecule shows six proton signals in the NMR spectrum, indicating its structural asymmetry. Intriguingly, despite its ostensively symmetric chemical structure, X-ray crystallography reveals that TPB lacks overall symmetry in its three-dimensional arrangement. This unexpected finding underscores the structural complexity of TPB and necessitates multifaceted examinations to elucidate its molecular properties.

We perform AIMD simulations to explore the structure and dynamics of TPB in the organic solvents  $CHCl_3$  and DMSO. In the DMSO solution, H2 and H4 atoms in the linker  $-CH_2$  groups exhibit probabilities exceeding 80% for forming intermolecular  $C-H\cdots O$  hydro-

gen bonds, making them less shielded from the C-H covalent bonds. In contrast, H1 and H3 orient towards the interior of the TPB molecule and are largely inaccessible to the DMSO solvents. As a result, the  $-\text{CH}_2$  chemical shifts manifest as two distributions and generate an additional proton signal in the <sup>1</sup>H NMR spectrum. Therefore, the interplay of structural asymmetry and solute-solvent C-H···O hydrogen bonds results in the observed chemical shift features in the <sup>1</sup>H NMR experiments. These finding provide a comprehensive understanding of the structure, symmetry and dynamical interactions of TPB in crystalline phase and organic solvents. The combined experimental and computational structural characterizations establish TPB's suitability as a reliable precursor for radiolabeling dimeric drugs. They lay the foundation for understanding the reaction of TPB with the <sup>18</sup>F<sup>-</sup> ion, which leads to the formation of [<sup>18</sup>F]5 and ultimately [<sup>18</sup>F]2b, as outlined in Figure 1. These insights are thus integral to the application of the molecule in the radiolabeling of dimeric drugs, which hold significant potentials as pharmaceutical and imaging agents. <sup>13,14,52,53</sup>

# Acknowledgement

L.W. acknowledges the support of the National Science Foundation through the award CHE-1904800. J.W. acknowledges the National Institutes of Health (NIH/NIA) for their support through grant K25AG061282. L.W. and Z.W. thank the Office of Advanced Research Computing at Rutgers University for providing access to the Amarel server.

# References

- (1) Paquin, A.; Reyes-Moreno, C.; Bérubé, G. Recent Advances in the Use of the Dimerization Strategy as a Means to Increase the Biological Potential of Natural or Synthetic Molecules. *Molecules* **2021**, *26*, 2340.
- (2) Nudelman, A. Dimeric Drugs. Curr. Med. Chem. 2022, 29, 2751–2845.

- (3) Berube, G. Natural and Synthetic Biologically Active Dimeric Molecules: Anticancer Agents, Anti-HIV Agents, Steroid Derivatives and Opioid Antagonists. *Curr. Med. Chem.* **2006**, *13*, 131–154.
- (4) Ren, Q.-C.; Gao, C.; Xu, Z.; Feng, L.-S.; Liu, M.-L.; Wu, X.; Zhao, F. Bis-coumarin Derivatives and Their Biological Activities. *Curr. Top. Med. Chem.* **2018**, *18*, 101–113.
- (5) Fröhlich, T.; Çapcı Karagöz, A.; Reiter, C.; Tsogoeva, S. B. Artemisinin-Derived Dimers: Potent Antimalarial and Anticancer Agents. J. Med. Chem. 2016, 59, 7360– 7388.
- (6) Shuker, S. B.; Hajduk, P. J.; Meadows, R. P.; Fesik, S. W. Discovering High-Affinity Ligands for Proteins: SAR by NMR. *Science* **1996**, *274*, 1531–1534.
- (7) Tamiz, A. P.; Zhang, J.; Zhang, M.; Wang, C. Z.; Johnson, K. M.; Kozikowski, A. P. Application of the Bivalent Ligand Approach to the Design of Novel Dimeric Serotonin Reuptake Inhibitors. J. Am. Chem. Soc. 2000, 122, 5393–5394.
- (8) Jencks, W. P. On the Attribution and Additivity of Binding Energies. *Proc. Natl. Acad. Sci. USA* **1981**, *78*, 4046–4050.
- (9) Mammen, M.; Choi, S.-K.; Whitesides, G. M. Polyvalent Interactions in Biological Systems: Implications for Design and Use of Multivalent Ligands and Inhibitors. Angew. Chem. Int. Ed. 1998, 37, 2754–2794.
- (10) Kramer, O. N.; Barkoff, M. S.; Hernandez, C. Mast Cell Activation Syndrome. *Skinmed* **2017**, *15*, 477—479.
- (11) Tefferi, A.; Pardanani, A. Systemic Mastocytosis: Current Concepts and Treatment Advances. *Curr. Hematol. Rep.* **2004**, *3*, 197—202.
- (12) Hori, Y.; Takeda, S.; Cho, H.; Wegmann, S.; Shoup, T. M.; Takahashi, K.; Irimia, D.; Elmaleh, D. R.; Hyman, B. T.; Hudry, E. A Food and Drug Administration-approved

- Asthma Therapeutic Agent Impacts Amyloid  $\beta$  in the Brain in a Transgenic Model of Alzheimer Disease. J. Biol. Chem. **2015**, 290, 1966–1978.
- (13) Shoup, T.; Normandin, M.; Takahashi, K.; Griciuc, A.; Dhaynaut, M.; Quinti, L.; Moon, S.-H.; Guehl, N.; Brugarolas, P.; Tanzi, R. E. et al. Fluorinated Cromolyn Derivatives for Potential Alzheimer's Disease Treatment. J. Nucl. Med. 2019, 60, 114.
- (14) Shoup, T. M.; Griciuc, A.; Normandin, M. D.; Quinti, L.; Walsh, L. V.; Dhaynaut, M.; Moon, S.-H.; Guehl, N. J.; Brugarolas, P.; Elmaleh, D. R. et al. Evaluation of Fluorinated Cromolyn Derivatives as Potential Therapeutics for Alzheimer's Disease. J. Alzheimers Dis. 2021, 80, 775–786, 2.
- (15) Elmaleh, D. R.; Shoup, T. Cromolyn derivatives and related methods of imaging and treatment. U.S. patent US 9,925,282 B2, 2018.
- (16) Case, D.; Belfon, K.; Ben-Shalom, I.; Brozell, S.; Cerutti, D.; Cheatham, T.; III; Cruzeiro, V.; Darden, T.; Duke, R. et al. Amber 2020. University of California: San Francisco, 2020.
- (17) Wang, J.; Wolf, R. M.; Caldwell, J. W.; Kollman, P. A.; Case, D. A. Development and testing of a general amber force field. *J. Comput. Chem.* **2004**, *25*, 1157–1174.
- (18) Loncharich, R. J.; Brooks, B. R.; Pastor, R. W. Langevin dynamics of peptides: The frictional dependence of isomerization rates of N-acetylalanyl-N-methylamide. *Biopoly*mers 1992, 32, 523–535.
- (19) Berendsen, H. J. C.; Postma, J. P. M.; van Gunsteren, W. F.; DiNola, A.; Haak, J. R. Molecular dynamics with coupling to an external bath. J. Chem. Phys. 1984, 81, 3684–3690.
- (20) Ryckaert, J.-P.; Ciccotti, G.; Berendsen, H. J. C. Numerical integration of the cartesian

- equations of motion of a system with constraints: molecular dynamics of n-alkanes. *J. Comput. Phys.* **1977**, *23*, 327–341.
- (21) Kühne, T. D.; Iannuzzi, M.; Del Ben, M.; Rybkin, V. V.; Seewald, P.; Stein, F.; Laino, T.; Khaliullin, R. Z.; Schütt, O.; Schiffmann, F. et al. CP2K: An electronic structure and molecular dynamics software package Quickstep: Efficient and accurate electronic structure calculations. J. Chem. Phys. 2020, 152, 194103.
- (22) Ceriotti, M.; More, J.; Manolopoulos, D. E. i-PI: A Python interface for ab initio path integral molecular dynamics simulations. Comput. Phys. Commun. 2014, 185, 1019– 1026.
- (23) Lee, C.; Yang, W.; Parr, R. G. Development of the Colle-Salvetti Correlation-Energy Formula into a Functional of the Electron Density. *Phys. Rev. B* **1988**, *37*, 785–789.
- (24) Becke, A. D. Density-functional exchange-energy approximation with correct asymptotic behavior. *Phys. Rev. A* **1988**, *38*, 3098.
- (25) Grimme, S.; Antony, J.; Ehrlich, S.; Krieg, H. A consistent and accurate ab initio parametrization of density functional dispersion correction (DFT-D) for the 94 elements H-Pu. J. Chem. Phys. 2010, 132, 154104.
- (26) Goedecker, S.; Teter, M.; Hutter, J. Separable dual-space Gaussian pseudopotentials. *Phys. Rev. B* **1996**, *54*, 1703–1710.
- (27) Godbout, N.; Salahub, D. R.; Andzelm, J.; Wimmer, E. Optimization of Gaussian-type basis sets for local spin density functional calculations. Part I. Boron through neon, optimization technique and validation. Can. J. Chem. 1992, 70, 560–571.
- (28) Bussi, G.; Donadio, D.; Parrinello, M. Canonical sampling through velocity rescaling. *J. Chem. Phys.* **2007**, *126*, 014101.

- (29) London, F. Théorie quantique des courants interatomiques dans les combinaisons aromatiques. J. Phys. Radium 1937, 8, 397–409.
- (30) McWeeny, R. Perturbation Theory for the Fock-Dirac Density Matrix. *Phys. Rev.* **1962**, 126, 1028–1034.
- (31) Ditchfield, R. Self-consistent perturbation theory of diamagnetism. *Mol. Phys.* **1974**, 27, 789–807.
- (32) Wolinski, K.; Hinton, J. F.; Pulay, P. Efficient implementation of the gauge-independent atomic orbital method for NMR chemical shift calculations. *J. Am. Chem. Soc.* **1990**, 112, 8251–8260.
- (33) Cheeseman, J. R.; Trucks, G. W.; Keith, T. A.; Frisch, M. J. A comparison of models for calculating nuclear magnetic resonance shielding tensors. *J. Chem. Phys.* **1996**, *104*, 5497–5509.
- (34) Frisch, M. J.; Trucks, G. W.; Schlegel, H. B.; Scuseria, G. E.; Robb, M. A.; Cheeseman, J. R.; Scalmani, G.; Barone, V.; Petersson, G. A.; Nakatsuji, H. et al. Gaussian 16 Revision A.03. Gaussian Inc. Wallingford CT, 2016.
- (35) Becke, A. D. Density-functional thermochemistry. III. The role of exact exchange. *J. Chem. Phys.* **1993**, *98*, 5648.
- (36) Stephens, P. J.; Devlin, F. J.; Chabalowski, C. F.; Frisch, M. J. Ab Initio Calculation of Vibrational Absorption and Circular Dichroism Spectra Using Density Functional Force Fields. J. Phys. Chem. 1994, 98, 11623–11627.
- (37) Lodewyk, M. W.; Siebert, M. R.; Tantillo, D. J. Computational Prediction of <sup>1</sup>H and <sup>13</sup>C Chemical Shifts: A Useful Tool for Natural Product, Mechanistic, and Synthetic Organic Chemistry. *Chem. Rev.* **2012**, *112*, 1839–1862.

- (38) Beran, G. J. eMagRes (eds R.K. Harris and R.L. Wasylishen); John Wiley Sons, Ltd, 2019; pp 215–226.
- (39) Venianakis, T.; Oikonomaki, C.; Siskos, M. G.; Primikyri, A.; Gerothanassis, I. P. DFT Calculations of 1H NMR Chemical Shifts of Geometric Isomers of Conjugated Linolenic Acids, Hexadecatrienyl Pheromones, and Model Triene-Containing Compounds: Structures in Solution and Revision of NMR Assignments. *Molecules* **2021**, *26*, 3477.
- (40) Desiraju, G. R. The CH···O Hydrogen Bond: Structural Implications and Supramolecular Design. Acc. Chem. Res. 1996, 29, 441–449.
- (41) Glendening, E. D.; Landis, C. R.; Weinhold, F. NBO 6.0: Natural bond orbital analysis program. *J. Comput. Chem.* **2013**, *34*, 1429–1437.
- (42) Hanson, R. M.; Prilusky, J.; Renjian, Z.; Nakane, T.; Sussman, J. L. JSmol and the Next-Generation Web-Based Representation of 3D Molecular Structure as Applied to Proteopedia. *Israel J. Chem.* 2013, 53, 207–216.
- (43) Marx, D.; Hutter, J. Ab Initio Molecular Dynamics: Basic Theory and Advanced Methods; Cambridge University Press, 2012.
- (44) Dračínský, M.; Möller, H. M.; Exner, T. E. Conformational Sampling by Ab Initio Molecular Dynamics Simulations Improves NMR Chemical Shift Predictions. J. Chem. Theory Comput. 2013, 9, 3806–3815.
- (45) Castro, A. C.; Balcells, D.; Repisky, M.; Helgaker, T.; Cascella, M. First-Principles Calculation of 1H NMR Chemical Shifts of Complex Metal Polyhydrides: The Essential Inclusion of Relativity and Dynamics. *Inorg. Chem.* 2020, 59, 17509–17518.
- (46) Zhou, S.; Wang, L. Symmetry and <sup>1</sup>H NMR chemical shifts of short hydrogen bonds: impact of electronic and nuclear quantum effects. *Phys. Chem. Chem. Phys.* **2020**, *22*, 4884–4895.

- (47) Mazurek, A. H.; Szeleszczuk, Ł.; Pisklak, D. M. A Review on Combination of Ab Initio Molecular Dynamics and NMR Parameters Calculations. *Int. J. Mol. Sci.* 2021, 22, 4378.
- (48) Maste, S.; Sharma, B.; Pongratz, T.; Grabe, B.; Hiller, W.; Erlach, M. B.; Kremer, W.; Kalbitzer, H. R.; Marx, D.; Kast, S. M. The accuracy limit of chemical shift predictions for species in aqueous solution. *Phys. Chem. Chem. Phys.* **2024**, *26*, 6386–6395.
- (49) Bondi, A. van der Waals Volumes and Radii. J. Phys. Chem. **1964**, 68, 441–451.
- (50) Hassanali, A. A.; Cuny, J. J.; Ceriotti, M.; Pickard, C. J.; Parrinello, M. The Fuzzy Quantum Proton in the Hydrogen Chloride Hydrates. *J. Chem. Am. Soc.* **2012**, *134*, 8557–8569.
- (51) Ceriotti, M.; Cuny, J.; Parrinello, M.; Manolopoulos, D. E. Nuclear quantum effects and hydrogen bond fluctuations in water. *Proc. Natl. Acad. Sci. USA* **2013**, *110*, 15591–6.
- (52) Guo, Z.; Gao, M.; Song, M.; Shi, C.; Zhang, P.; Xu, D.; You, L.; Zhuang, R.; Su, X.; Liu, T. et al. Synthesis and Evaluation of <sup>99m</sup>Tc-Labeled Dimeric Folic Acid for FR-Targeting. *Molecules* **2016**, *21*, 817.
- (53) Wang, J.; Qu, X.; Shoup, T. M.; Yuan, G.; Afshar, S.; Pan, C.; Zhu, A.; Choi, J.-K.; Kang, H. J.; Poutiainen, P. et al. Synthesis and Characterization of Fluorine-18-Labeled N-(4-Chloro-3-((fluoromethyl-d2)thio)phenyl)picolinamide for Imaging of mGluR4 in Brain. J. Med. Chem. 2020, 63, 3381–3389.